

Vacuum-gap-based lumped element Josephson parametric amplifier

Sishi Wu(吴思诗), Dengke Zhang(张登科), Rui Wang(王锐), Yulong Liu(刘玉龙), Shuai-Peng Wang(王帅鹏), Qichun Liu(刘其春), J S Tsai(蔡兆申), and Tiefu Li(李铁夫)

Citation: Chin. Phys. B, 2022, 31 (**1**): 010306. DOI: 10.1088/1674-1056/ac280c
Journal homepage: http://cpb.iphy.ac.cn; http://iopscience.iop.org/cpb

What follows is a list of articles you may be interested in

Disorder in parity-time symmetric quantum walks

Peng Xue(薛鹏)
Chin. Phys. B, 2022, 31 (**1**): 010311. DOI: 10.1088/1674-1056/ac3741

Optimized pulse for stimulated Raman adiabatic passage on noisy experimental platform

Zhi-Ling Wang(王志凌), Leiyinan Liu(刘雷轶男), and Jian Cui(崔健)
Chin. Phys. B, 2021, 30 (**8**): 080305. DOI: 10.1088/1674-1056/abfccb

Quantum computation and simulation with superconducting qubits

Kaiyong He(何楷泳), Xiao Geng(耿霄), Rutian Huang(黄汝田), Jianshe Liu(刘建设), and Wei Chen(陈炜)
Chin. Phys. B, 2021, 30 (**8**): 080304. DOI: 10.1088/1674-1056/ac16cf

Universal quantum control based on parametric modulation in superconducting circuits

Dan-Yu Li(李丹宇), Ji Chu(储继), Wen Zheng(郑文), Dong Lan(兰栋), Jie Zhao(赵杰), Shao-Xiong Li(李邵雄), Xin-Sheng Tan(谭新生), and Yang Yu(于扬)
Chin. Phys. B, 2021, 30 (**7**): 070308. DOI: 10.1088/1674-1056/ac01c3

Nb-based Josephson parametric amplifier for superconducting qubit measurement

Fei-Fan Su(宿非凡), Zi-Ting Wang(王子婷), Hui-Kai Xu(徐晖凯), Shou-Kuan Zhao(赵寿宽), Hai-Sheng Yan(严海生), Zhao-Hua Yang(杨钊华), Ye Tian(田野), Shi-Ping Zhao(赵士平)
Chin. Phys. B, 2019, 28 (**11**): 110303. DOI: 10.1088/1674-1056/ab4578

Vacuum-gap-based lumped element Josephson parametric amplifier

Sishi Wu(吴思诗)[1], Dengke Zhang(张登科)[2,3], Rui Wang(王锐)[2,3], Yulong Liu(刘玉龙)[4,†], Shuai-Peng Wang(王帅鹏)[1], Qichun Liu(刘其春)[4], J S Tsai(蔡兆申)[2,3], and Tiefu Li(李铁夫)[4,5,‡]

[1] *Quantum Physics and Quantum Information Division, Beijing Computational Science Research Center, Beijing* 100193, *China*
[2] *Department of Physics, Tokyo University of Science, Kagurazaka, Shinjuku-ku, Tokyo* 162-8601, *Japan*
[3] *RIKEN Center for Quantum Computing (RQC),* 2-1 *Hirosawa, Wako, Saitama* 351-0198, *Japan*
[4] *Beijing Academy of Quantum Information Sciences, Beijing* 100193, *China*
[5] *School of Integrated Circuits, and Frontier Science Center for Quantum Information, Tsinghua University, Beijing* 100084, *China*

(Received 8 June 2021; revised manuscript received 19 August 2021; accepted manuscript online 18 September 2021)

We propose a lumped element Josephson parametric amplifier with vacuum-gap-based capacitor. The capacitor is made of quasi-floating aluminum pad and on-chip ground. We take a fabrication process compatible with air-bridge technology, which makes our design adaptable for future on-chip integrated quantum computing system. Further engineering the input impedance, we obtain a gain above 20 dB over 162-MHz bandwidth, along with a quasi quantum-limit noise performance. This work should facilitate the development of quantum information processing and integrated superconducting circuit design.

Keywords: Josephson parametric amplifier, vacuum gap, quantum-limit noise

PACS: 03.67.Lx, 85.25.Cp, 74.50.+r **DOI:** 10.1088/1674-1056/ac280c

1. Introduction

Parametric amplifiers are mostly pumped nonlinear oscillators, among which Josephson parametric amplifier (JPA) is a primary candidate for superconducting circuits.[1–6] Josephson junctions provide not only lossless non-linearity but also the flexibility of working points. In the last decades, Josephson junctions have been employed to realize the quantum-limited parametric amplifier, which plays quite important roles in, *e.g.*, single-shot readout,[7–9] quantum state squeezing,[10,11] and quantum jump trajectory.[12] With the emerging of noisy intermediate-scale superconducting quantum technology (NISQ),[13–15] wide bandwidth amplifiers with quasi quantum-limit noise are quite in demand for fault-tolerant quantum computing.

The mainstream of existing wide bandwidth JPA can be sorted into traveling-wave-based and lumped-element-based types. On the aspect of gain response, traveling wave parametric amplifiers (TWPAs)[16–18] typically provide gain above 10 dB with bandwidth of several-Gigahertz, while lumped element Josephson parametric amplifiers (LJPAs)[19–22] commonly have 100-MHz bandwidth accompanied with gain of 20 dB. On the fabrication aspect, TWPAs need reliable fabrication for series of thousands of Josephson junctions, and LJPAs are composed by superconducting quantum interference device (SQUID) and lumped capacitor, like interdigitated capacitor,[22] and parallel-plate capacitor.[23–25] It is worth noting that, to preserve working region, capacitors with small parasitic inductance, such as parallel-plate capacitor and vacuum-gap-based capacitor, are preferred. While parallel-plate capacitor lowers parasitic inductance of the interdigitated capacitor, its multi-layer structure introduces fabrication complexity and amorphous heterogeneous interface, where surface defects are most likely to be found. Although most JPA devices have declared quasi quantum-limit noise, further decreasing defects makes a considerable difference on qubit readout fidelity, which is a key limitation for current scalability of quantum computing.

Typical wideband LJPA design takes comparatively large lumped element capacitance, and skips coupling capacitors to the environment. These lead to wider spectral linewidth, but smaller impedance, due to the limitation of characteristic frequency. To lower impedance mismatch at the signal reflection interface, impedance transformers becomes a common choice, among which, coplanar waveguide (CPW) based one is a primary candidate for its simple designable structure.[26–29] Commonly used CPW-based impedance transformers are composed of a quarter-wavelength CPW section (with main characteristic parameters including resonant frequency $\omega_{\rm q}$ and impedance $Z_{\rm q}$) and a half-wavelength CPW section (with $\omega_{\rm h}$ and $Z_{\rm h}$). According to transmission line theory, input impedance of a load can be transformed via CPW section, which can be expressed as $Z_{\rm in}(\omega_{\rm s}) = Z_{\rm cpw}\{Z_{\rm L} + {\rm i}Z_{\rm cpw}\tan(2\pi\bar{\nu}\omega_{\rm s}/\omega_{\rm cpw})\}/\{Z_{\rm cpw} + {\rm i}Z_{\rm L}\tan(2\pi\bar{\nu}\omega_{\rm s}/\omega_{\rm cpw})\}$. The variables labeled with 'cpw' refer to parameters of the CPW section, $Z_{\rm L}$ refers to load impedance, and $\omega_{\rm s}$ refers to probe signal frequency.[26] There-

†Corresponding author. E-mail: liuyl@baqis.ac.cn
‡Corresponding author. E-mail: litf@tsinghua.edu.cn

© 2022 Chinese Physical Society and IOP Publishing Ltd

fore, for $\omega_s \approx \omega_{cpw}$, quarter-wavelength CPW section (with $\bar{\nu} = 1/4$) edits the real part of the input impedance, and half-wavelength CPW section (with $\bar{\nu} = 1/2$) balances the imaginary part. Introduction of auxiliary impedance engineering helps break gain-bandwidth product limitation of LJPA to be several-hundred-Megahertz bandwidth accompanied with gain about 20 dB.[23,30,31]

In this paper, we propose an LJPA with vacuum-gap-based capacitor. Aluminum-based microelectronic processing is adopted, which means the design can be integrated for Josephson-junction-based on-chip superconducting quantum computing system. The lumped capacitor using vacuum-gap-based structure results in lower parasitic inductance and smaller amorphous heterogeneous interface.[32] The separated superconducting pads are patterned via photo lithography, while the quasi-floating one requires extra evaporation and wet etching. Multi-material fabrication, including amorphous silicon,[21,23,31] silicon nitride,[31] or silicon oxide[30] to form capacitor gaps are avoided. Pad size is designed comparatively larger, in order to certificate structural ductility and process reliability of the vacuum-gap-based capacitor. Additionally, the device is strongly coupled to the environment via a CPW-based impedance transformer to increase gain bandwidth.[26,27]

2. Theory

In the perspective of theoretical analysis, the Josephson junctions embedded circuit can be treated as nonlinear cavity. With external pump, circuit Hamiltonian can be mapped onto a parametric amplifier.[4,5,33,34] For typical wide-band weak signal gain usage, to avoid pump tone interfering, JPAs are pumped around twice the frequency of its eigen-mode, which refers to the so called three-wave mixing. Three wave mentioned here are named as pump tone (ω_d), probe tone (ω_s), and idler tone (ω_i), with serial characteristic frequencies satisfying $\omega_d = \omega_s + \omega_i$ (See Fig. 1). The Hamiltonian can be written as

$$H = \hbar\widetilde{\Delta}_r(a_s^\dagger a_s + a_i^\dagger a_i) - i\hbar\lambda(a_s a_i - a_s^\dagger a_i^\dagger), \tag{1}$$

where a_s ($a_s^\dagger$) and a_i ($a_i^\dagger$) are annihilation (creation) operators for probe and idler tones. $\widetilde{\Delta}_r = \omega_r - \omega_d/2 - 2\lambda$, with λ representing the effective driving strength, and ω_r representing the nonlinear cavity frequency. λ is meanly determined by the Kerr constant and averaged intra-cavity photon number, which is dominated by the strong pump. In our design, lumped element parameters are of $C_{vgb} = 4.83$ pF (capacitance of the vacuum-gap-based part), $L_{vgb} = 24.2$ pH (parasitic inductance of the vacuum-gap-based part) and $L_S[0] = 165$ pH (unbiased inductance of the SQUID).

Combination of quantum Langevin equation and input-output theory gives the photon number gain of the probe tone $G[\omega_s]$, which is indeed the square of modulus of the reflection coefficient:[16,35]

$$G[\omega_s] = |1 - \kappa\chi_{11}|^2, \tag{2}$$

where χ_{11} is an element of system susceptibility matrix $\chi[\omega_s]$, which arises from $[a_s, a_i]^T = \chi[\omega_s][a_{s,in}, a_{i,in}]^T$. And κ is the effective damping rate, dependent by both the JPA intrinsic damping rate and the impedance difference of it from the environment. While the former factor is determined by the vacuum-gap-based capacitor and the SQUID, the latter can be lowered by impedance engineering, and thus broadens the JPA gain bandwidth.

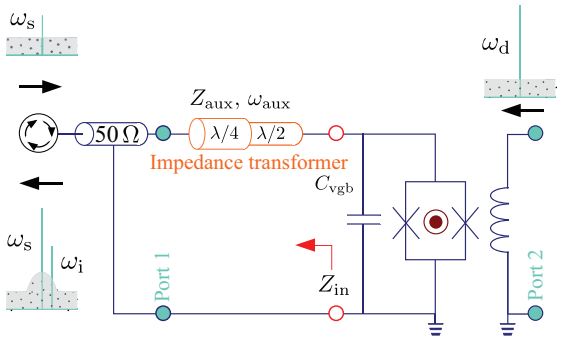


Fig. 1. Illustration of components for the LJPA device, including CPW-based impedance transformer, vacuum-gap-based lumped capacitor and SQUID. During the three wave mixing process, annihilation of a pump tone photon comes with creation of a probe tone photon and an idler tone photon, and *vice versa*.

For the specific circuit presented in this work (see Fig. 2), with auxiliary CPW-based impedance transformer, effective damping rate can be approximated into $1/(2C_{vgb}R_t)$, when the probe tone is slightly detuned from $\omega_d/2$. The transformed environment resistance is of $R_t = Z_q^2/R$, where $Z_q = 40.9\ \Omega$ is impedance of the quarter-wavelength CPW transformer, a partial auxiliary impedance engineering part, and $R = 50\ \Omega$ is resistance of the input channel. Resonant frequencies of quarter-wavelength CPW transformer and half-wavelength CPW transformer are designed to be $\omega_q = \omega_h = 5.6$ GHz, which is mainly determined by the length of the waveguides. Besides, Z_q is designed to be $58.0\ \Omega$. Impedance of the waveguides is mainly determined by the width of the centerline and gap. Accordingly, the system susceptibility matrix $\chi[\omega_s]$ can be expressed as[21,27]

$$\chi[\omega_s] = \begin{pmatrix} -i(\omega_d - \omega_s) + \frac{Y_{in}^*[\omega_s]}{2C_{vgb}} & \lambda \\ \lambda & -i\omega_s + \frac{Y_{in}[\omega_d - \omega_s]}{2C_{vgb}} \end{pmatrix}^{-1}. \tag{3}$$

The input admittance $Y_{in}[\omega_s]$ can be expressed as $(R_t + iZ_{aux}\omega_s/\omega_{aux})^{-1}$. While R_t meanly determines expansion of the spectral bandwidth, mismatch of $iZ_{aux}\omega_s/\omega_{aux}$ and standing wave emerged in the cable, produce ripple on the reflected spectrum. According to transmission line theory,[26,27] the total auxiliary CPW transformer (seen from the lumped part) has impedance of $Z_{aux} = \{Z_q(1 - Z_q^2/R^2) + 2Z_h[1 - Z_q^4/(R^2Z_h^2)]\} \times$

$\pi/4 = 71.4\ \Omega$ and frequency of $\omega_{\rm aux}/2\pi = 5.6$ GHz. Note that for large detuning, approximation of self-energy terms into $Y^*_{\rm in}[\omega_{\rm s}]/(2C_{\rm vgb})$ and $Y_{\rm in}[\omega_{\rm d}-\omega_{\rm s}]/(2C_{\rm vgb})$ should be adjusted. For the optimal pump power at certain pump frequency, the gain response spectral can be approximately given[25,27] as

$$G[\omega_{\rm s}] = G_{\rm max}/\{1+(\Delta_{\rm s}/\Gamma_{\rm BW})^4\}, \tag{4}$$

where $\Delta_{\rm s} = \omega_{\rm d}/2 - \omega_{\rm s}$, $G_{\rm max} = 1 + 16\kappa^2\lambda^2/\{\kappa^2 - 4\lambda^2 + 4(\omega_{\rm r} - \omega_{\rm d}/2)^2\}^2$, and $\Gamma_{\rm BW} = \kappa/(2G_{\rm max}^{1/4})$. Such broadened lineshape comes as higher order approximation of Taylor expansion for Eq. (2), due to the enlarged $\kappa/2\pi = 0.49$ GHz.

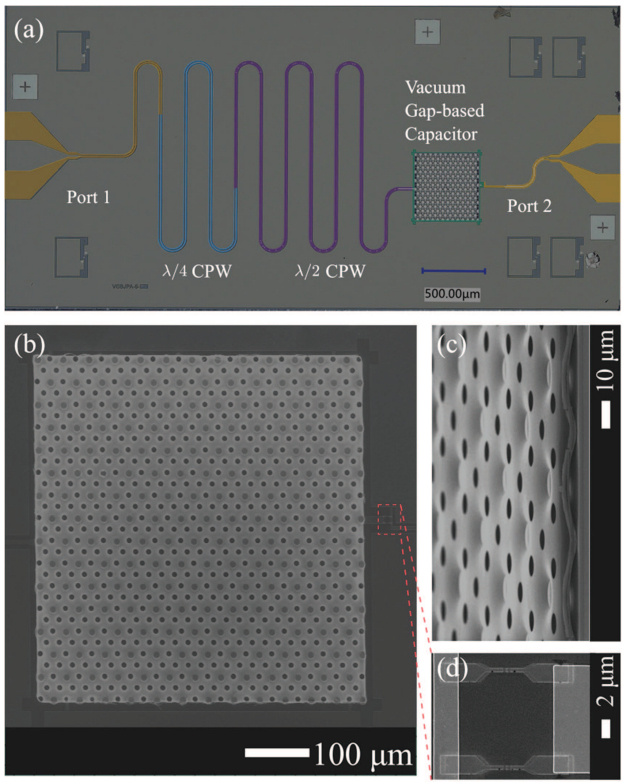


Fig. 2. Photos of the vacuum-gap-based lumped element Josephson parametric amplifier. (a) An optical image of the whole structure, which is characterized in this paper. The circuit components are individually colored and labeled. Port 1 is made for microwave signal, including probe tone and direct pump tone. Port 2 is made for both microwave signal and direct current input, thus allowing flux pump and on-chip bias. (b) A SEM image of the whole vacuum-gap-based structure and SQUID. The lighter larger rounds are standing contacts to support the floating pad. The darker small holes are made for removing the sacrifice layer during fabrication. (c) A SEM image of partial lumped capacitor, which serves as a proof of the quasi-floating condition. (d) A SEM image of the fabricated SQUID.

3. Design and fabrication

The structure of our LJPA is composed of lumped element part, CPW-based impedance transforming part, and control line. The lumped element part is composed of vacuum-gap-based capacitor and SQUID. The control line is designed to allow both microwave pump and flux bias.

Fabrication process[32,36] is illustrated in Fig. 3. On-chip lumped capacitor pad, control line and impedance engineering part are firstly patterned via photo lithography and dry etching from a niobium sputtered silicon substrate. Standing contacts of the lumped capacitor are separated from the on-chip ground by concentric ring gaps. CPW-based impedance transformer and SQUID are directly connected to the quasi-floating pad through standing contacts. Then we use e-beam lithography followed with double angle evaporation and in-chamber oxidation to fabricate the Josephson junctions. Another round of photo lithography is applied to reserve standing contacts between the on-chip ground and the quasi-floating capacitor pad. The photon resist (thickness about 3 μm) used here serves as sacrifice layer. The quasi-floating capacitor pad is then formed by aluminum evaporation, and is separated from the on-chip one by initially etched gaps. Wet etching after third round of photo lithography is taken, to remove photon resist sacrifice layer and unwanted aluminum part. Both standing contacts and top layer etched holes are designed as regular hexagon nested array.

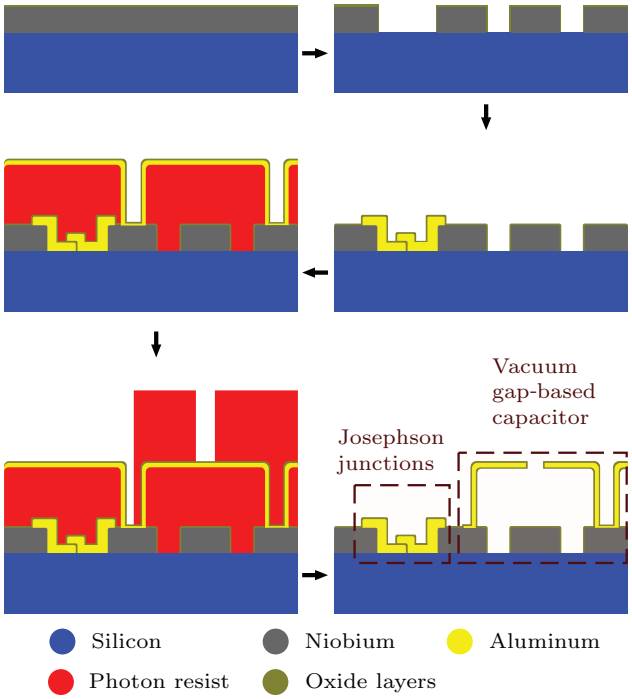


Fig. 3. Fabrication process for the vacuum-gap-based JPA. The circuit element sizes are distortedly plotted for illustrations. Material types are marked by different colors and annotated.

4. Measurement and results

Our characterization measurement is taken at 25 mK in a dilution refrigerator. Weak probe tone with characteristic frequency of $\omega_{\rm s}$, is injected by the network analyzer through port 1. It experiences attenuation before reaching to the cryogenic environment. A circulator is placed in front of port 1. The pump tone is applied by signal generator through port 2. Mixing process transfer energy from the strong pump tone to the weak probe tone. The amplified probe tone then comes out, together with the idler tone and noise, through the circulator.

The flux bias on the SQUID loop is controlled by global coil inside the magnetic shield, which can be replaced by flux input through on-chip control line, together with flux pump, using bias-tee. Spectrum analyzer is added into the output channel, to analyze the device noise performance.

Firstly, we modulate JPA characteristic frequency by applying flux to the SQUID loop through an external coil. Flexibility of circuit characteristic frequency allows Gigahertz-range operational bandwidth. As is illustrated in Fig. 4, gain region is not restrict to the frequency of CPW transformer, because its coupling to both environment and JPA is strong. However, expansion of gain bandwidth for signal dispersive from $\omega_{\rm aux}$ is weakened.

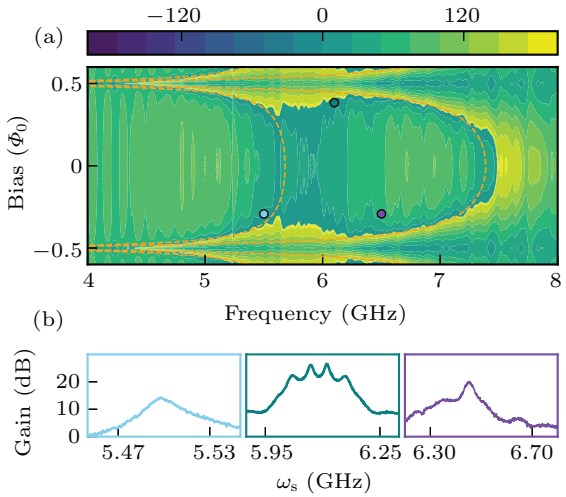


Fig. 4. Bias-dependent reflection spectrum. (a) Unpumped phase spectrum for varied bias. Orange dash line is the characteristic frequency fitting of the CPW transformer dressed JPA circuit. Φ_0 refers to flux quanta. Three biased points are marked in blue, green, and purple. Their accordingly three wave mixing stimulated gain spectrum is plotted below. (b) The blue spectrum is pumped at 11 GHz, and biased at $-0.293\Phi_0$. The green spectrum is pumped at 12.18 GHz, and biased at $0.404\Phi_0$. The purple spectrum is pumped at 13 GHz, and biased at $-0.292\Phi_0$.

We then focus on bias at $0.404\Phi_0$, to characterize performance of the device. Under the pump tone with frequency of 12.18 GHz and power of −108 dBm, we obtain over 20-dB gain with 162-MHz bandwidth. The corresponding 1-dB compression is about −123 dBm. Measurement results indicate the capability for simultaneous multi-qubit readout. Note that all amplitudes of input signals are described in the amount before reaching sample box. Dynamic range and gain bandwidth of the device can be optimized by adjusting size of the vacuum-gap-based capacitor.[37] If size of the vacuum-gap-based capacitor is halved, which results in halved $C_{\rm vgb}$, similar to the JPAs with dielectric layer based parallel-plate capacitor,[31] gain bandwidth should be broadened beyond 300 MHz. Meanwhile, dynamic range should be decreased for the same nonlinear cavity frequency targeted design.[33]

We then compare the spectrum analyzer detected signal to noise ratio (SNR) under pumped and unpumped cases, for which subplot in Fig. 5(d) serves as an example. With accordance to the characterized input channel attenuation and gain response (exactly the blue line in Fig. 5(c)), this gives the JPA noise.

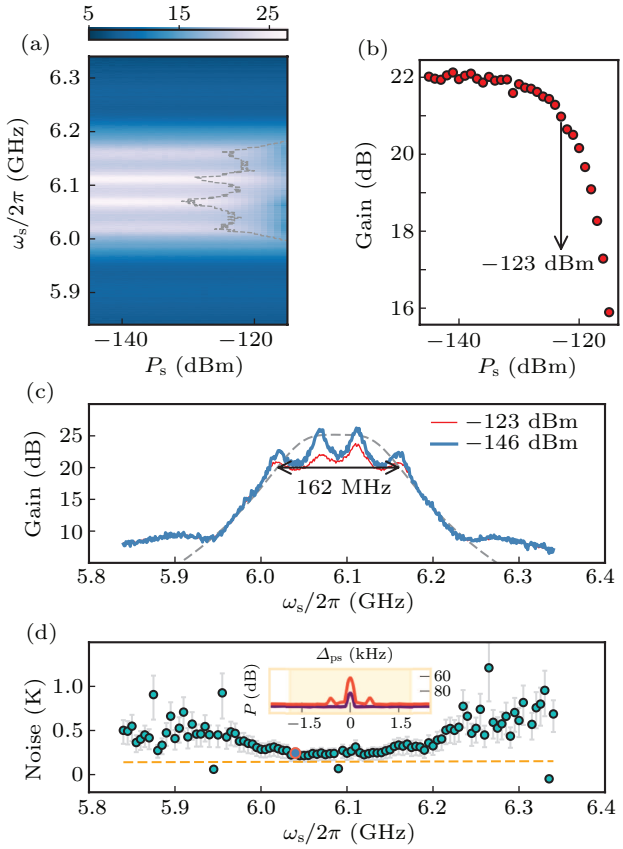


Fig. 5. LJPA performance characterization under pump condition of 12.18 GHz, −108 dBm. (a) Gain response evolution toward saturation along growing probe tone amplitude, for series probe frequencies. Probe frequency dependent 1-dB compression is plotted as gray dash line. (b) Detailed plot of the left one, for probe frequency at 6.09 GHz, with marked 1-dB compression at −123 dBm. (c) Gain response for probe power at −146 dBm (blue line) and −123 dBm (red line). Gray dash line represents gain response lineshape fitting. (d) Measured JPA noise (dots), with 1.2-dB insertion loss error colored in gray, and orange dash line indicating quantum limit. Frequency-dependent noise photon number is transferred into noise temperature via $\hbar\omega/k_{\rm B}$. Processing of SNR, at input signal frequency of 6.04 GHz, is taken as an example (circled in pink). Its original data ($Q_{\rm out}[\tau] = \int_{-1/2\tau}^{1/2\tau} P[\Delta_{\rm ps}]\,{\rm d}\Delta_{\rm ps}$) zoomed in 5 kHz span is presented in the subplot, where the pink area refers to integration period τ (1/3.75 kHz), and $\Delta_{\rm ps}$ refers to frequency difference between probe tone and swept signal tone. T is the sufficiently settled integration period for wideband fast Fourier transformation that covers the JPA gain bandwidth (1/100 kHz). Red line refers to the pumped spectrum, and purple line refers to the unpumped spectrum. SNR is thus concluded from $Q_{\rm out}[\tau](T-\tau)/\{\tau(N_{\rm tot}[T]-Q_{\rm out}[\tau])\}$, where $N_{\rm tot}[T] = \int_{-1/2T}^{1/2T} P[\Delta_{\rm ps}]\,{\rm d}\Delta_{\rm ps}$.

To be specific, we can have a system noise in unit of quanta defined as

$$N = Q_{\rm in}[\tau]/{\rm SNR}, \tag{5}$$

where footlabel 'in (out)' on $Q[\tau]$ refers to signal photon number input (output) during an integration period of τ, and SNR represents signal to noise ratio detected by the frequency spectrum analyzer. It is worth-noting that integration period influence little on the noise calculation, because it is contained

both in numerator and denominator of SNR. When JPA is not pumped,

$$\mathrm{SNR}_{\mathrm{up}} = Q_{\mathrm{s}}[\tau]/N_{\mathrm{a}}[\tau], \tag{6}$$

where footlabel 'up (p)' on SNR refers to the unpumped (pumped) condition, Q_{s} means the fixed injected probe tone photon number (around 2000), and N_{a} means noise added by the output channel with high electron mobility transistor (HEMT) and room temperature amplifier. Similarly, when JPA is pumped, we have

$$N_{\mathrm{tot}} = N_{\mathrm{j}} + N_{\mathrm{a}}/G_{\mathrm{j}}, \tag{7a}$$

$$\mathrm{SNR}_{\mathrm{p}} = \frac{G_{\mathrm{j}}(Q_{\mathrm{s}}[\tau] + N_{\mathrm{j}}[\tau]) + N_{\mathrm{a}}[\tau]}{N_{\mathrm{a}}[\tau] + G_{\mathrm{j}}N_{\mathrm{j}}[\tau]}, \tag{7b}$$

where N_{j} means noise added by the JPA, and G_{j} means JPA gain. Comparing $\mathrm{SNR}_{\mathrm{p}}$ and $\mathrm{SNR}_{\mathrm{up}}$ gives

$$N_{\mathrm{j}} = \frac{Q_{\mathrm{in}}}{\mathrm{SNR}_{\mathrm{p}} - 1} - \frac{Q_{\mathrm{s}}}{G_{\mathrm{j}}\mathrm{SNR}_{\mathrm{up}}}. \tag{8}$$

This thermal calibration source free method well matched the widely taken approximation method, where the noise is expressed as $T_{\mathrm{JPA}}[\omega] = T_{\mathrm{tot}}[\omega](1/\eta_{\mathrm{SNR}}[\omega] - 1/G[\omega])$.[22] In this formula, $T_{\mathrm{tot\,(JPA)}}$ means the total (JPA) added noise in the temperature scale, η_{SNR} means SNR improvement, and G means JPA gain. Noise measurement results confirm that the vacuum-gap-based structure reaches quasi quantum-limit.

5. Conclusion

For rounds of cooling, robustness of the vacuum-gap-based geometric structure has been verified. We also varied the gap design to test their room temperature capacitance, which turns to have parallel-plate-capacitor-equivalent linear dependency on size. This confirms designability of the electrical parameters.

In summary, we have proposed a vacuum-gap-based capacitance structure for fabricating low-noise lumped element JPA, with single material evaporation method. Our JPA achieves over 20-dB gain with 162-MHz bandwidth, with added noise about 1 quanta. The circuit can be further optimized by finite impedance engineering and smaller capacitor. Our device offers application in single-shot readout of multi-qubit system, which emerges with the coming NISQ era.

Toward future integrated superconducting quantum circuits, air-bridge is becoming an essential component. Due to the fabrication compatibility, our vacuum-gap-based LJPA can be a strong candidate for hardware-efficient on-chip amplification. The vacuum-gap-based structure also inspires 3D-architectures of superconducting circuits. Furthermore, such capacitor with low parasitic inductance can play roles in lumped element circuit to tailor local electric field distribution, which offers flexibility on designing characteristic frequency and coupling strength.

Acknowledgements

Project supported by the National Key Research and Development Program of China (Grant No. 2016YFA0301200), the National Natural Science Foundation of China (Grant Nos. 62074091, 12004044, and U1930402), the Science Challenge Project (Grant No. TZ2018003), the Fund from the New Energy and Industrial Technology Development Organization (Grant No. JPNP16007), and Japan Science and Technology Agency (Moonshot R&D, Grant No. JPMJMS2067 and CREST, Grant No. JPMJCR1676).

References

[1] Zimmer H 1967 *Appl. Phys. Lett.* **10** 193
[2] Yurke B, Corruccini L, Kaminsky P, Rupp L, Smith A, Silver A, Simon R and Whittaker E 1989 *Phys. Rev. A* **39** 2519
[3] Yamamoto T, Inomata K, Watanabe M, Matsuba K, Miyazaki T, Oliver W D, Nakamura Y and Tsai J 2008 *Appl. Phys. Lett.* **93** 042510
[4] Clerk A A, Devoret M H, Girvin S M, Marquardt F and Schoelkopf R J 2010 *Rev. Mod. Phys.* **82** 1155
[5] Laflamme C and Clerk A A 2011 *Phys. Rev. A* **83** 033803
[6] Wendin G 2017 *Rep. Prog. Phys.* **80** 106001
[7] Lin Z, Inomata K, Oliver W, Koshino K, Nakamura Y, Tsai J and Yamamoto T 2013 *Appl. Phys. Lett.* **103** 132602
[8] Schaal S, Ahmed I, Haigh J, Hutin L, Bertrand B, Barraud S, Vinet M, Lee C M, Stelmashenko N, Robinson J, *et al.* 2020 *Phys. Rev. Lett.* **124** 067701
[9] Crescini N, Alesini D, Braggio C, Carugno G, D Agostino D, Di Gioacchino D, Falferi P, Gambardella U, Gatti C, Iannone G, *et al.* 2020 *Phys. Rev. Lett.* **124** 171801
[10] Castellanos-Beltran M A, Irwin K D, Hilton G C, *et al.* 2008 *Nat. Phys.* **4** 929
[11] Eichler C, Bozyigit D, Lang C, Baur M, Steffen L, Fink J, Filipp S and Wallraff A 2011 *Phys. Rev. Lett.* **107** 113601
[12] Riste D, Dukalski M, Watson C, De Lange G, Tiggelman M, Blanter Y M, Lehnert K W, Schouten R and DiCarlo L 2013 *Nature* **502** 350
[13] Preskill J 2018 *Quantum* **2** 79
[14] Arute F, Arya K, Babbush R, Bacon D, Bardin J C, Barends R, Biswas R, Boixo S, Brandao F G, Buell D A, *et al.* 2019 *Nature* **574** 505
[15] Jurcevic P, Javadi-Abhari A, Bishop L S, *et al.* 2021 *Quantum Sci. Technol.* **6** 025020
[16] Zhou X, Schmitt V, Bertet P, Vion D, Wustmann W, Shumeiko V and Estève D 2014 *Phys. Rev. B* **89** 214517
[17] Macklin C, O brien K, Hover D, Schwartz M, Bolkhovsky V, Zhang X, Oliver W and Siddiqi I 2015 *Science* **350** 307
[18] Zorin A 2019 *Phys. Rev. Appl.* **12** 044051
[19] Hatridge M, Vijay R, Slichter D, Clarke J and Siddiqi I 2011 *Phys. Rev. B* **83** 134501
[20] Mutus J Y, White T C, Jeffrey E, Sank D, Barends R, Bochmann J, Chen Y, Chen Z, Chiaro B, Dunsworth A, *et al.* 2013 *Appl. Phys. Lett.* **103** 122602
[21] Mutus J Y, White T C, Barends R, Chen Y, Chen Z, Chiaro B, Dunsworth A, Jeffrey E, Kelly J, Megrant A, *et al.* 2014 *Appl. Phys. Lett.* **104** 263513
[22] Elo T, Abhilash T, Perelshtein M, Lilja I, Korostylev E and Hakonen P 2019 *Appl. Phys. Lett.* **114** 152601
[23] Huang K, Guo Q, Song C, Zheng Y, Deng H, Wu Y, Jin Y, Zhu X and Zheng D 2017 *Chin. Phys. B* **26** 094203

[24] Bockstiegel C, Gao J, Vissers M, Sandberg M, Chaudhuri S, Sanders A, Vale L, Irwin K and Pappas D 2014 *J. Low Temp. Phys.* **176** 476

[25] Duan P, Jia Z, Zhang C, *et al.* 2021 *Appl. Phys. Express* **14** 042011

[26] Pozar D M 2012 *Microwave Engineering* (New York: John Wiley & Sons) pp. 26–30

[27] Roy T, Kundu S, Chand M, Vadiraj A, Ranadive A, Nehra N, Patankar M P, Aumentado J, Clerk A and Vijay R 2015 *Appl. Phys. Lett.* **107** 262601

[28] Su F F, Wang Z T, Xu H K, Zhao S K, Yan H S, Yang Z H, Tian Y and Zhao S P 2019 *Chin. Phys. B* **28** 110303

[29] Lu Y P, Zuo Q, Pan J Z, *et al.* 2021 *Chin. Phys. B* **30** 068504

[30] Xue H, Lin Z, Jiang W, Niu Z, Liu K, Peng W and Wang Z 2021 *Chin. Phys. B* **30** 068503

[31] Grebel J, Bienfait A, Dumur É, Chang H S, Chou M H, Conner C, Peairs G, Povey R, Zhong Y and Cleland A 2021 *Appl. Phys. Lett.* **118** 142601

[32] Cicak K, Li D, Strong J A, Allman M S, Altomare F, Sirois A J, Whittaker J D, Teufel J D and Simmonds R W 2010 *Appl. Phys. Lett.* **96** 093502

[33] Eichler C and Wallraff A 2014 *EPJ Quantum Technol.* **1** 1

[34] Yurke B and Buks E 2006 *J. Light Technol.* **24** 5054

[35] Krantz P, Reshitnyk Y, Wustmann W, Bylander J, Gustavsson S, Oliver W D, Duty T, Shumeiko V and Delsing P 2013 *New J. Phys.* **15** 105002

[36] Chen Z, Megrant A, Kelly J, Barends R, Bochmann J, Chen Y, Chiaro B, Dunsworth A, Jeffrey E, Mutus J, *et al.* 2014 *Appl. Phys. Lett.* **104** 052602

[37] Wustmann W and Shumeiko V 2013 *Phys. Rev. B* **87** 184501